Precision Measurement of the Proton Flux in Primary Cosmic Rays from Rigidity 1 GV to 1.8 TV with the Alpha Magnetic Spectrometer on the International Space Station

M. Aguilar,[26] D. Aisa,[33,34] B. Alpat,[33] A. Alvino,[33] G. Ambrosi,[33] K. Andeen,[22] L. Arruda,[24] N. Attig,[21] P. Azzarello,[33,16] A. Bachlechner,[1] F. Barao,[24] A. Barrau,[17] L. Barrin,[15] A. Bartoloni,[38] L. Basara,[3,37] M. Battarbee,[45] R. Battiston,[37,a] J. Bazo,[33] U. Becker,[9] M. Behlmann,[9] B. Beischer,[1] J. Berdugo,[26] B. Bertucci,[33,34] G. Bigongiari,[35,36] V. Bindi,[19] S. Bizzaglia,[33] M. Bizzarri,[33,34] G. Boella,[28,29] W. de Boer,[22] K. Bollweg,[20] V. Bonnivard,[17] B. Borgia,[38,39] S. Borsini,[33] M. J. Boschini,[28] M. Bourquin,[16] J. Burger,[9] F. Cadoux,[16] X. D. Cai,[9] M. Capell,[9] S. Caroff,[3] J. Casaus,[26] V. Cascioli,[33] G. Castellini,[14] I. Cernuda,[26] D. Cerreta,[33,34] F. Cervelli,[35] M. J. Chae,[41] Y. H. Chang,[10] A. I. Chen,[9] H. Chen,[9] G. M. Cheng,[6] H. S. Chen,[6] L. Cheng,[42] H. Y. Chou,[10] E. Choumilov,[9] V. Choutko,[9] C. H. Chung,[1] C. Clark,[20] R. Clavero,[23] G. Coignet,[3] C. Consolandi,[19] A. Contin,[7,8] C. Corti,[19] E. Cortina Gil,[16,b] B. Coste,[37,15] W. Creus,[10] M. Crispoltoni,[33,34] Z. Cui,[42] Y. M. Dai,[5] C. Delgado,[26] S. Della Torre,[28] M. B. Demirköz,[2] L. Derome,[17] S. Di Falco,[35] L. Di Masso,[33,34] F. Dimiccoli,[37] C. Díaz,[26] P. von Doetinchem,[19] F. Donnini,[33,34] W. J. Du,[42] M. Duranti,[33,34] D. D'Urso,[33] A. Eline,[9] F. J. Eppling,[9] T. Eronen,[45] Y. Y. Fan,[44,c] L. Farnesini,[33] J. Feng,[3,d] E. Fiandrini,[33,34] A. Fiasson,[3] E. Finch,[32] P. Fisher,[9] Y. Galaktionov,[9] G. Gallucci,[35] B. García,[26] R. García-López,[23] C. Gargiulo,[15] H. Gast,[1] I. Gebauer,[22] M. Gervasi,[28,29] A. Ghelfi,[17] W. Gillard,[10] F. Giovacchini,[26] P. Goglov,[9] J. Gong,[31] C. Goy,[3] V. Grabski,[27] D. Grandi,[28] M. Graziani,[33,34] C. Guandalini,[7,8] I. Guerri,[35,36] K. H. Guo,[18] D. Haas,[16,e] M. Habiby,[16] S. Haino,[10,44] K. C. Han,[25] Z. H. He,[18] M. Heil,[9] J. Hoffman,[10] T. H. Hsieh,[9] Z. C. Huang,[18] C. Huh,[13] M. Incagli,[35] M. Ionica,[33,34] W. Y. Jang,[13] H. Jinchi,[25] K. Kanishev,[37,15] G. N. Kim,[13] K. S. Kim,[13] Th. Kirn,[1] R. Kossakowski,[3] O. Kounina,[9] A. Kounine,[9] V. Koutsenko,[9] M. S. Krafczyk,[9] G. La Vacca,[28] E. Laudi,[33,34,f] G. Laurenti,[7,8] I. Lazzizzera,[37] A. Lebedev,[9] H. T. Lee,[44] S. C. Lee,[44] C. Leluc,[16] G. Levi,[7,8] H. L. Li,[44,g] J. Q. Li,[31] Q. Li,[31] Q. Li,[9,h] T. X. Li,[18] W. Li,[4] Y. Li,[16,d] Z. H. Li,[6] Z. Y. Li,[44,d] S. Lim,[13] C. H. Lin,[44] P. Lipari,[38] T. Lippert,[21] D. Liu,[44] H. Liu,[31] M. Lolli,[7,8] T. Lomtadze,[35] M. J. Lu,[37,i] S. Q. Lu,[44,d] Y. S. Lu,[6] K. Luebelsmeyer,[1] J. Z. Luo,[31] S. S. Lv,[18] R. Majka,[32] C. Mañá,[26] J. Marín,[26] T. Martin,[20] G. Martínez,[26] N. Masi,[7,8] D. Maurin,[17] A. Menchaca-Rocha,[27] Q. Meng,[31] D. C. Mo,[18] L. Morescalchi,[35,j] P. Mott,[20] M. Müller,[1] J. Q. Ni,[18] N. Nikonov,[22] F. Nozzoli,[33] P. Nunes,[24] A. Obermeier,[1] A. Oliva,[26] M. Orcinha,[24] F. Palmonari,[7,8] C. Palomares,[26] M. Paniccia,[16] A. Papi,[33] M. Pauluzzi,[33,34] E. Pedreschi,[35] S. Pensotti,[28,29] R. Pereira,[19] N. Picot-Clemente,[12] F. Pilo,[35] A. Piluso,[33,34] C. Pizzolotto,[33] V. Plyaskin,[9] M. Pohl,[16] V. Poireau,[3] E. Postaci,[2] A. Putze,[3,k] L. Quadrani,[7,8] X. M. Qi,[18] X. Qin,[33,g] Z. Y. Qu,[44,l] T. Räihä,[1] P. G. Rancoita,[28] D. Rapin,[16] J. S. Ricol,[17] I. Rodríguez,[26] S. Rosier-Lees,[3] A. Rozhkov,[9] D. Rozza,[28] R. Sagdeev,[11] J. Sandweiss,[32] P. Saouter,[16] C. Sbarra,[7,8] S. Schael,[1] S. M. Schmidt,[21] A. Schulz von Dratzig,[1] G. Schwering,[1] G. Scolieri,[33] E. S. Seo,[12] B. S. Shan,[4] Y. H. Shan,[4] J. Y. Shi,[31] X. Y. Shi,[9,m] Y. M. Shi,[43] T. Siedenburg,[1] D. Son,[13] F. Spada,[38] F. Spinella,[35] W. Sun,[9] W. H. Sun,[9,n] M. Tacconi,[28,29,15] C. P. Tang,[18] X. W. Tang,[6] Z. C. Tang,[6] L. Tao,[3] D. Tescaro,[23] Samuel C. C. Ting,[9] S. M. Ting,[9] N. Tomassetti,[17] J. Torsti,[45] C. Türkoğlu,[2] T. Urban,[20] V. Vagelli,[22] E. Valente,[38,39] C. Vannini,[35] E. Valtonen,[45] S. Vaurynovich,[9] M. Vecchi,[40] M. Velasco,[26] J. P. Vialle,[3] V. Vitale,[33] S. Vitillo,[16] L. Q. Wang,[42] N. H. Wang,[42] Q. L. Wang,[5] R. S. Wang,[43] X. Wang,[9] Z. X. Wang,[18] Z. L. Weng,[9] K. Whitman,[19] J. Wienkenhöver,[1] H. Wu,[31] X. Wu,[16] X. Xia,[26,g] M. Xie,[9,h] S. Xie,[43] R. Q. Xiong,[31] G. M. Xin,[42] N. S. Xu,[18] W. Xu,[6,9] Q. Yan,[9] J. Yang,[41] M. Yang,[6] Q. H. Ye,[43] H. Yi,[31] Y. J. Yu,[5] Z. Q. Yu,[6] S. Zeissler,[22] J. H. Zhang,[31] M. T. Zhang,[18] X. B. Zhang,[18] Z. Zhang,[18] Z. M. Zheng,[4] H. L. Zhuang,[6] V. Zhukov,[1] A. Zichichi,[7,8] N. Zimmermann,[1] P. Zuccon,[9] and C. Zurbach[30]

(AMS Collaboration)

[1]*I. Physics Institute and JARA-FAME, RWTH Aachen University, D-52056 Aachen, Germany*
[2]*Department of Physics, Middle East Technical University (METU), 06800 Ankara, Turkey*
[3]*Laboratoire d'Annecy–le–Vieux de Physique des Particules (LAPP), IN2P3/CNRS and Université de Savoie Mont Blanc, F-74941 Annecy-le-Vieux, France*
[4]*Beihang University (BUAA), Beijing 100191, China*
[5]*Institute of Electrical Engineering (IEE), Chinese Academy of Sciences, Beijing 100190, China*
[6]*Institute of High Energy Physics (IHEP), Chinese Academy of Sciences, Beijing 100039, China*
[7]*INFN Sezione di Bologna, I-40126 Bologna, Italy*
[8]*Università di Bologna, I-40126 Bologna, Italy*
[9]*Massachusetts Institute of Technology (MIT), Cambridge, Massachusetts 02139, USA*
[10]*National Central University (NCU), Chung-Li, Tao Yuan 32054, Taiwan*
[11]*East-West Center for Space Science, University of Maryland, College Park, Maryland 20742, USA*

[12]IPST, University of Maryland, College Park, Maryland 20742, USA
[13]CHEP, Kyungpook National University, 702-701 Daegu, Korea
[14]CNR–IROE, I-50125 Firenze, Italy
[15]European Organization for Nuclear Research (CERN), CH-1211 Geneva 23, Switzerland
[16]DPNC, Université de Genève, CH-1211 Genève 4, Switzerland
[17]Laboratoire de Physique Subatomique et de Cosmologie (LPSC), CNRS/IN2P3 and Université Grenoble–Alpes, F-38026 Grenoble, France
[18]Sun Yat–Sen University (SYSU), Guangzhou 510275, China
[19]Physics and Astronomy Department, University of Hawaii, Honolulu, Hawaii 96822, USA
[20]National Aeronautics and Space Administration Johnson Space Center (JSC), and Jacobs-Sverdrup, Houston, Texas 77058, USA
[21]Jülich Supercomputing Centre and JARA-FAME, Research Centre Jülich, D-52425 Jülich, Germany
[22]Institut für Experimentelle Kernphysik, Karlsruhe Institute of Technology (KIT), D-76128 Karlsruhe, Germany
[23]Instituto de Astrofísica de Canarias (IAC), E-38205 La Laguna, and Departamento de Astrofísica, Universidad de La Laguna, E-38206 La Laguna, Tenerife, Spain
[24]Laboratório de Instrumentação e Física Experimental de Partículas (LIP), P-1000 Lisboa, Portugal
[25]National Chung–Shan Institute of Science and Technology (NCSIST), Longtan, Tao Yuan 325, Taiwan
[26]Centro de Investigaciones Energéticas, Medioambientales y Tecnológicas (CIEMAT), E-28040 Madrid, Spain
[27]Instituto de Física, Universidad Nacional Autónoma de México (UNAM), México, D. F. 01000, Mexico
[28]INFN Sezione di Milano–Bicocca, I-20126 Milano, Italy
[29]Università di Milano–Bicocca, I-20126 Milano, Italy
[30]Laboratoire Univers et Particules de Montpellier (LUPM), IN2P3/CNRS and Université de Montpellier II, F-34095 Montpellier, France
[31]Southeast University (SEU), Nanjing 210096, China
[32]Physics Department, Yale University, New Haven, Connecticut 06520, USA
[33]INFN Sezione di Perugia, I-06100 Perugia, Italy
[34]Università di Perugia, I-06100 Perugia, Italy
[35]INFN Sezione di Pisa, I-56100 Pisa, Italy
[36]Università di Pisa, I-56100 Pisa, Italy
[37]INFN TIFPA and Università di Trento, I-38123 Povo, Trento, Italy
[38]INFN Sezione di Roma 1, I-00185 Roma, Italy
[39]Università di Roma La Sapienza, I-00185 Roma, Italy
[40]Instituto de Fìsica de São Carlos, Universidade de São Paulo, CP 369, 13560-970 São Carlos, São Paulo, Brazil
[41]Department of Physics, Ewha Womans University, Seoul 120-750, Korea
[42]Shandong University (SDU), Jinan, Shandong 250100, China
[43]Shanghai Jiaotong University (SJTU), Shanghai 200030, China
[44]Institute of Physics, Academia Sinica, Nankang, Taipei 11529, Taiwan
[45]Space Research Laboratory, Department of Physics and Astronomy, University of Turku, FI-20014 Turku, Finland

(Received 6 March 2015; published 30 April 2015)

A precise measurement of the proton flux in primary cosmic rays with rigidity (momentum/charge) from 1 GV to 1.8 TV is presented based on 300 million events. Knowledge of the rigidity dependence of the proton flux is important in understanding the origin, acceleration, and propagation of cosmic rays. We present the detailed variation with rigidity of the flux spectral index for the first time. The spectral index progressively hardens at high rigidities.

DOI: 10.1103/PhysRevLett.114.171103 PACS numbers: 98.70.Sa, 95.55.Vj, 95.85.Ry, 96.50.sb

Protons are the most abundant charged particles in cosmic rays. Knowledge of the precise behavior of the proton spectrum is important in understanding the origin, acceleration, and propagation of cosmic rays [1]. Recent important measurements of the proton flux in cosmic rays have reported different variations of the flux with energy [2–6]. These measurements generated widespread interest. In particular, the ATIC–2, CREAM, and PAMELA experiments showed deviations of the proton flux from a single power law. Many models were proposed to account for the hardening of the flux based on different sources, acceleration mechanisms, diffusive propagation effects, and their superposition [7]. In this Letter we report on the precise measurement of the proton flux in primary cosmic rays in the rigidity range from 1 GV to 1.8 TV based on data collected by the Alpha Magnetic Spectrometer (AMS)

during the first 30 months (May 19, 2011 to November 26, 2013) of operation onboard the International Space Station (ISS).

Detector.—AMS is a general purpose high energy particle physics detector in space. The layout and description of the detector are presented in Ref. [8]. The key elements used in this measurement are the permanent magnet, the silicon tracker, four planes of time of flight (TOF) scintillation counters, and the array of anticoincidence counters (ACCs). AMS also contains a transition radiation detector (TRD), a ring imaging Čerenkov detector (RICH), and an electromagnetic calorimeter (ECAL). The three-dimensional imaging capability of the 17 radiation length ECAL allows for an accurate measurement of the $e^{\pm}$ energy E and of the shower shape.

The AMS coordinate system is concentric with the magnet. The x axis is parallel to the main component of the magnetic field and the z axis points vertically. The (y-z) plane is the bending plane. Above, below, and downward-going refer to the AMS coordinate system.

The central field of the magnet [9] is 1.4 kG. Before flight, the field was measured in 120 000 locations to an accuracy of better than 2 G. On orbit, the magnet temperature varies from -3 to $+15°$ C. The field strength is corrected with a measured temperature dependence of $-0.09\%/°$C.

The tracker [10] has nine layers, the first (L1) at the top of the detector, the second (L2) just above the magnet, six (L3 to L8) within the bore of the magnet, and the last (L9) just above the ECAL. L2 to L8 constitute the inner tracker. Each layer contains double-sided silicon microstrip detectors which independently measure the x and y coordinates. The tracker accurately determines the trajectory of cosmic rays by multiple measurements of the coordinates with a resolution in each layer of 10 μm in the bending (y) direction. The inner tracker is held stable by a carbon fiber structure with negligible coefficient of thermal expansion. The stability of the inner tracker is monitored using 20 IR laser beams which penetrate layers L2 through L8 and provide submicron position measurements. Using cosmic rays over a 2 minute window, the position of L1 is aligned with a precision of 5 μm with respect to the inner tracker and L9 with a precision of 6 μm. Together, the tracker and the magnet measure the rigidity R of charged cosmic rays. The maximum detectable rigidity (MDR) is 2 TV over the 3 m lever arm from L1 to L9.

Each layer of the tracker also provides an independent measurement of the absolute value of the charge $|Z|$ of the cosmic ray. The charge resolution of the layers of the inner tracker together is $\Delta Z \simeq 0.05$ for $|Z| = 1$ particles.

Two planes of TOF counters [11] are located above L2 and two planes are located below the magnet. For $|Z| = 1$ particles, the average time resolution of each counter has been measured to be 160 ps and the overall velocity ($\beta = v/c$) resolution to be $\Delta\beta/\beta^2 = 4\%$. This discriminates between upward- and downward-going particles.

The coincidence of signals from the four TOF planes together with the absence of signals from the ACC provides a charged particle trigger. The ACC has an efficiency of 0.999 99 to reject cosmic rays which enter the inner tracker from the side. The coincidence of 3 out of the 4 TOF layers with no ACC requirement was used to provide an unbiased trigger. The unbiased trigger, prescaled by 1%, was used to measure the efficiency of the charged particle trigger. The efficiency of the unbiased trigger was estimated directly from the data to be above 99.8% for all rigidities using events in which one of the four TOF layers gave no signal. This allowed the estimation of the efficiency of each TOF layer and, consequently, the efficiency of the unbiased trigger.

Before launch, at the CERN SPS, AMS was extensively calibrated with 180 and 400 GeV/c proton beams and beams of positrons, electrons, and pions from 10 to 290 GeV/c. In total, calibrations with 18 different energies and particles at 2000 positions were performed. These data allow the determination of the tracker rigidity resolution function with high precision and the verification of the absolute rigidity scale.

Since launch, the detector has been monitored and controlled around the clock. The time, location, and orientation are provided by GPS units affixed to AMS and to the ISS. The detector performance has been steady over time.

Simulated events were produced using a dedicated program developed by the collaboration from the GEANT-4.9.6 package [12] based on Monte Carlo methods. This program simulates electromagnetic and hadronic interactions of particles in the material of AMS and generates detector responses. The digitization of the signals is simulated precisely according to the measured characteristics of the electronics. The simulated events then undergo the same reconstruction as used for the data. Figure 1 shows a comparison of the inverse rigidity for 400 GeV/c protons from the test beam and the Monte Carlo simulation. As

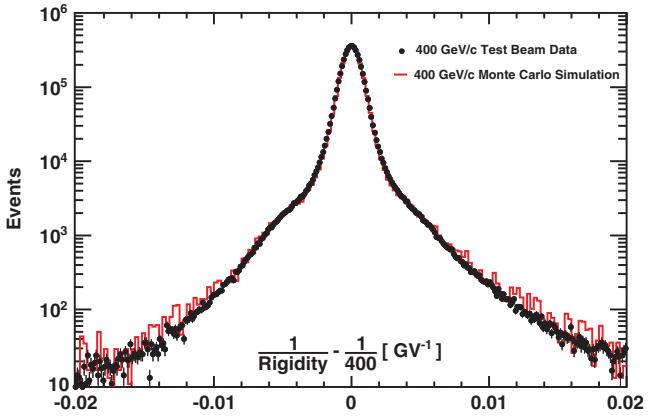

FIG. 1 (color). The resolution function in inverse rigidity for 400 GeV/c protons measured in the test beam compared with the Monte Carlo simulation.

seen, the resolution has a pronounced Gaussian core with non-Gaussian tails of ~5% and the simulation precisely reproduces the measured resolution including the tails.

Selection.—In the first 30 months (7.96×10^7 s) AMS collected 4.1×10^{10} cosmic ray events. The effective data collection time includes only those seconds during which the detector was in normal operating conditions, the AMS z axis was within 40° of the local zenith, the trigger live time exceeded 50%, and the ISS was outside of the South Atlantic Anomaly. Because of the influence of the geomagnetic field, this collection time for primary cosmic rays increases with increasing rigidity becoming constant at 6.29×10^7 s above 30 GV.

By selecting events to be downward going and to have a reconstructed track in the inner tracker with $|Z| = 1$, we obtain 1.1×10^{10} events. In order to have the best resolution at the highest rigidities, further selections are made by requiring the track to pass through L1 and L9 and to satisfy additional track fitting quality criteria such as a $\chi^2/d.f. < 10$ in the bending coordinate. Then positively charged particles are selected. In addition, to select only primary cosmic rays, well above the geomagnetic cutoff, the measured rigidity is required to be greater than 1.2 times the maximum geomagnetic cutoff within the AMS field of view. The cutoff was calculated by backtracing [13] particles from the top of AMS out to 50 Earth's radii using the International Geomagnetic Reference Field (IGRF) [14]. Finally, the small contamination of low energy (below 2 GeV) pions produced in the upper part of the detector is removed by requiring that the mass, determined by combining the velocity measured by the TOF with the rigidity, of the selected particle is larger than 0.5 GeV/c^2. These procedures resulted in a sample of 3.0×10^8 primary cosmic rays with $Z = +1$.

Since protons are the dominant component of cosmic rays, the selected sample of 3.0×10^8 events has only small contributions of other particles, mainly deuterons. The deuteron contribution decreases with rigidity; at 1 GV it is less than 2% and at 20 GV it is 0.6% [15,16]. Deuterons were not removed. The sample also contains protons from nuclei which interact at the top of AMS (for example, in L1 or the TRD). From the measured flux [17] and Monte Carlo simulation this contribution is 0.5% at 1 GV decreasing to less than 0.1% at and above 10 GV. Contamination from e^+ and e^- [18], overwhelmingly e^+, was estimated to be less than 0.1% over the entire rigidity range. The background contributions from protons which originated in the interactions of nuclei at the top of AMS and $e^{\pm}$, both noticeable only below 2 GV, are subtracted from the flux and the uncertainties are accounted for in the systematic errors.

Analysis.—The isotropic proton flux Φ_i for the ith rigidity bin $(R_i, R_i + \Delta R_i)$ is

$$\Phi_i = \frac{N_i}{A_i \epsilon_i T_i \Delta R_i}, \tag{1}$$

where N_i is the number of events corrected with the rigidity resolution function (see below), A_i is the effective acceptance, ϵ_i is the trigger efficiency, and T_i is the collection time. In this Letter the proton flux was measured in 72 bins, $i = 1$ to 72, from 1 GV to 1.8 TV with bin widths chosen according to the rigidity resolution. The effective acceptance A_i was calculated using Monte Carlo simulation and then corrected for small differences found between the data and Monte Carlo event selection efficiencies. The trigger efficiency ϵ_i is measured from data with the unbiased trigger events. The trigger efficiency ranges from 90% to 95%. The 5% to 10% inefficiency is due to secondary δ rays in the magnetic field entering the ACC. The Monte Carlo simulation agrees with the measured trigger efficiency within 0.5%.

The bin-to-bin migration of events was corrected using a rigidity resolution function obtained from Monte Carlo simulation and verified with the test beam data, see for example Fig. 1. Among many unfolding procedures, we selected two. The validity of both were verified by our Monte Carlo simulation. In the first procedure the flux is obtained iteratively [19]. Initially, the flux is evaluated using Eq. (1) without taking the rigidity resolution function into account. Subsequently, at each iteration, the folded acceptance A' is calculated for each bin, $A'_i = (1/\Phi_i)\sum_j \Phi_j A_j M_{ij}$, where M_{ij} is the migration matrix obtained from the rigidity resolution function. Next, A' is parametrized using a spline function. Finally, the number of events is corrected bin by bin by a factor A/A' and the flux is reevaluated using Eq. (1). The iteration proceeds until the fluxes between two successive steps agree within 0.1%. The results in this Letter are based on this procedure. The second procedure is based on a forward unfolding technique [20]. A set of spline functions with different node positions is used to parametrize the corrected number of events per bin. The spline functions are folded with the migration matrix M_{ij} and fit to the data. The average of those spline functions compatible with data is used to obtain N_i. The small differences between the two procedures ($< 0.5\%$) are accounted for as a systematic error. We have checked the sensitivity of the results to the binning by increasing the bin width by factors of 2 and 4 as well as reducing the bin width by factors of 2 and 4. The resulting uncertainty is well within the assigned systematic errors.

Extensive studies were made of the systematic errors. The errors include the uncertainties in the trigger efficiency, the acceptance, the background contamination, the geomagnetic cutoff factor, the event selection, the unfolding, the rigidity resolution function, and the absolute rigidity scale. The trigger efficiency error is dominated by the statistics available from the 1% prescaled unbiased event sample. It is negligible (less than 0.4%) below 500 GV and reaches 1.5% at 1.8 TV. The geomagnetic cutoff factor was varied from 1.0 to 1.4 and the resulting proton fluxes

showed a systematic uncertainty of 2% at 1 GV and negligible above 2 GV. We have also verified that using the most recent IGRF model [21] and the IGRF model with external nonsymmetric magnetic fields [22] does not introduce observable changes in the flux values nor in the systematic errors.

The effective acceptance was corrected for small differences between the data and the Monte Carlo samples related to the event reconstruction and selection. Together, the correction was found to be 5% at 1 GV decreasing below 2% above 10 GV, while the corresponding systematic uncertainty is less than 1.5% above 2 GV.

The detector is mostly made of carbon and aluminum. The corresponding inelastic cross sections of $p+\mathrm{C}$ and $p+\mathrm{Al}$ are known to within 10% at 1 GV and 4% at 300 GV [23], and 7% at 1.8 TV from model estimations [12]. The inelastic cross sections are used in the Monte Carlo calculation of the effective acceptance and, to estimate the systematic error due to the uncertainty in the inelastic cross sections, dedicated samples of protons were simulated with the $p+\mathrm{C}$ and $p+\mathrm{Al}$ cross sections varied by $\pm 10\%$. From the analysis of these samples together with the current knowledge of the cross sections, systematic errors of 1% at 1 GV, 0.6% from 10 to 300 GV, and 0.8% at 1.8 TV were obtained.

The rigidity resolution function was verified with data from both the ISS and the test beam. For this the residuals between the hit coordinates measured in tracker layers L1 and L9 and those obtained from the track fit using the information from only the inner tracker L2 to L8 were compared between data and simulation. In order to validate the alignment of the external layers the difference between the rigidity measured using the information from L1 to L8 and from L2 to L9 was compared between data and the simulation. The resulting uncertainty on the MDR was estimated to be 5%. The corresponding unfolding errors were obtained by varying the width of the Gaussian core of the resolution function by 5% and the amplitude of the non-Gaussian tails by ~20% (see for example Fig. 1) over the entire rigidity range and found to be 1% below 200 GV and 3% at 1.8 TV.

There are two contributions to the systematic uncertainty on the rigidity scale. The first is due to residual tracker misalignment. From the 400 GeV/c test beam data it was measured to be less then $1/300\ \mathrm{TV}^{-1}$. For the ISS data, this error was estimated by comparing the E/p ratio for electron and positron events, where E is the energy measured with the ECAL and p is the momentum measured with the tracker, see Ref. [24] for details. It was found to be $1/26\ \mathrm{TV}^{-1}$, limited by the current high energy positron statistics. The second systematic error on the rigidity scale arises from the magnetic field map uncertainties (0.25%) and temperature correction uncertainties (0.1%). Taken in quadrature and weighted by the rigidity dependence of the flux, this amounts to a systematic error on the flux of less than 0.5% for rigidities above 2 GV.

To ensure that the treatment of systematic errors described above is correct, we performed several additional, independent verifications. Figure 2 shows examples of the stability of the measured flux for different conditions (presented as the ratio to the average flux). Figure 2(a) shows the dependence of the integral of the proton flux above 30 GV, i.e., above the maximum geomagnetic cutoff, on the angle θ between the incoming proton direction and the AMS z axis; this verifies the systematic error assigned to the acceptance. Figure 2(b) shows the monthly integral flux above 45 GV is within the systematic error of 0.4%.

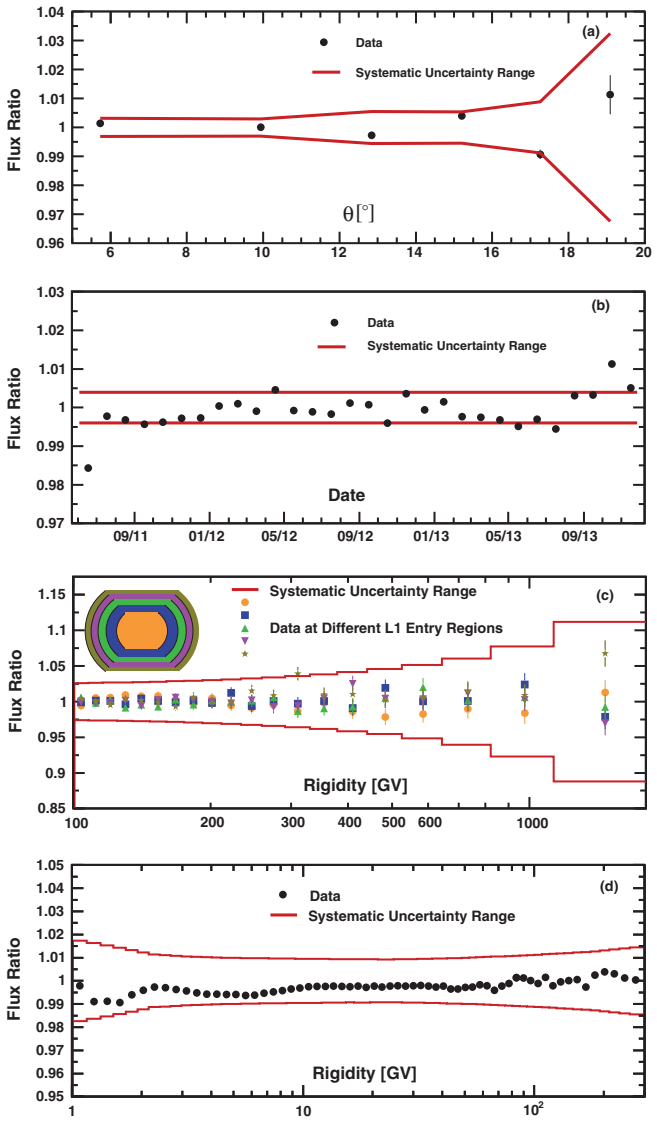

FIG. 2 (color). Independent verification of the systematic errors. The curves indicate the corresponding systematic errors. (a) The variation of the flux ratio above 30 GV vs the angle θ to the AMS z axis. (b) The variation of the flux ratio above 45 GV vs time. (c) The variation of the flux ratio vs the rigidity for different L1 entry regions (see inset). (d) The variation of the flux ratio measured using only the inner tracker (L2 to L8) vs the full tracker (L1 to L9).

This verifies that the detector performance is stable over time and that the flux above 45 GV shows no observable effect from solar modulation fluctuations for this measurement period. The variation of the proton flux due to solar modulation will be the subject of a separate publication. Figure 2(c) shows that the ratios of fluxes obtained using events which pass through different sections of L1 to the average flux are in good agreement and within the assigned systematic errors; this verifies the errors assigned to the tracker alignment. Lastly, as seen from Fig. 2(d), the flux obtained using the rigidity measured by only the inner tracker is in good agreement with the flux measured using the full lever arm; this verifies the systematic errors assigned from the unfolding procedures and the rigidity resolution function for two extreme and important cases. First, at the inner tracker MDR (~300 GV) where the unfolding effects and resolution functions of the inner tracker and the full lever arm (2 TV MDR) are very different. Second, at low rigidities (1 to 10 GV) where the unfolding effects and the tails in the resolution functions of the inner tracker and full lever arm are also very different due to large multiple and nuclear scattering.

Most importantly, several independent analyses were performed on the same data sample by different study groups. The results of those analyses are consistent with this Letter.

Results.—The measured proton flux Φ including statistical errors and systematic errors is tabulated in Ref. [25] as a function of the rigidity at the top of the AMS detector. The contributions to the systematic errors come from (i) the trigger, (ii) the acceptance, background contamination, geomagnetic cutoff, and event selection, (iii) the rigidity resolution function and unfolding, and (iv) the absolute rigidity scale. The contributions of individual sources to the systematic error are added in quadrature to arrive at the total systematic uncertainty. The Monte Carlo event samples have sufficient statistics such that they do not contribute to the errors. Figure 3(a) shows the flux as a function of rigidity with the total errors, the sum in quadrature of statistical and systematic errors [26]. In this and the subsequent figures, the points are placed along the abscissa at $\tilde{R}$ calculated for a flux $\propto R^{-2.7}$ [27]. Figure 3(b) shows the AMS flux as a function of kinetic energy E_K together with the most recent results (i.e., from experiments after the year 2000).

A power law with a constant spectral index γ

$$\Phi = CR^{\gamma} \tag{2}$$

where R is in GV and C is a normalization factor, does not fit the flux reported in this work [25] and shown in Fig. 3(a) at the 99.9% C.L. for $R > 45$ GV. Applying solar modulation in the force field approximation [28] also does not fit the data at the 99.9% C.L. for $R > 45$ GV. We therefore fit the flux with a modified spectral index [29]

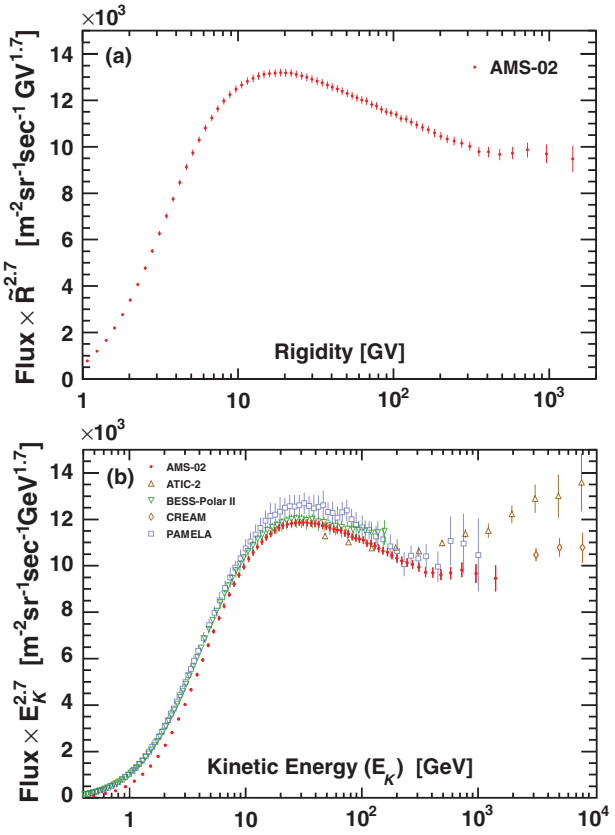

FIG. 3 (color). (a) The AMS proton flux multiplied by $\tilde{R}^{2.7}$ and the total error as a function of rigidity. (b) The flux as a function of kinetic energy E_K as multiplied by $E_K^{2.7}$ compared with recent measurements [3–6]. For the AMS results $E_K \equiv \sqrt{\tilde{R}^2 + M_p^2} - M_p$ where M_p is the proton mass.

$$\Phi = C\left(\frac{R}{45\ \mathrm{GV}}\right)^{\gamma}\left[1 + \left(\frac{R}{R_0}\right)^{\Delta\gamma/s}\right]^{s}, \tag{3}$$

where s quantifies the smoothness of the transition of the spectral index from γ for rigidities below the characteristic transition rigidity R_0 to $\gamma + \Delta\gamma$ for rigidities above R_0. Fitting over the range 45 GV to 1.8 TV yields a $\chi^2/d.f. = 25/26$ with $C = 0.4544 \pm 0.0004(\mathrm{fit})^{+0.0037}_{-0.0047}(\mathrm{sys})^{+0.0027}_{-0.0025}$ (sol) $\mathrm{m^{-2}sr^{-1}sec^{-1}GV^{-1}}$, $\gamma = -2.849 \pm 0.002(\mathrm{fit})^{+0.004}_{-0.003}$ $(\mathrm{sys})^{+0.004}_{-0.003}(\mathrm{sol})$, $\Delta\gamma = 0.133^{+0.032}_{-0.021}(\mathrm{fit})^{+0.046}_{-0.030}(\mathrm{sys}) \pm 0.005(\mathrm{sol})$, $s = 0.024^{+0.020}_{-0.013}(\mathrm{fit})^{+0.027}_{-0.016}(\mathrm{sys})^{+0.006}_{-0.004}(\mathrm{sol})$, and $R_0 = 336^{+68}_{-44}(\mathrm{fit})^{+66}_{-28}(\mathrm{sys}) \pm 1(\mathrm{sol})$ GV. The first error quoted (fit) takes into account the statistical and uncorrelated systematic errors from the flux reported in this work [25]. The second (sys) is the error from the remaining systematic errors, namely, from the rigidity resolution function and unfolding, and from the absolute rigidity scale, with their bin-to-bin correlations accounted for using the migration matrix M_{ij}. The third (sol) is the uncertainty due to the variation of the solar potential $\phi = 0.50$ to 0.62 GV [30]. The fit confirms that above 45 GV the flux is

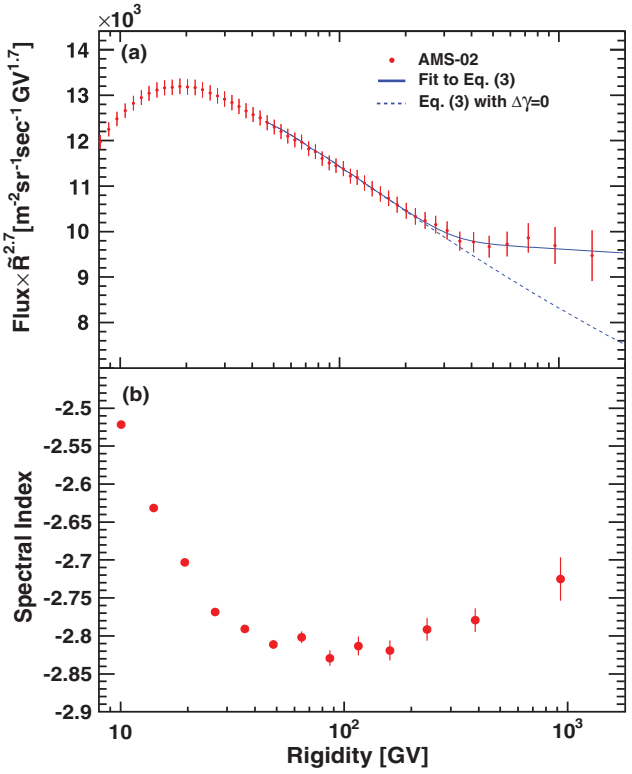

FIG. 4 (color). (a) The AMS proton flux multiplied by $\tilde{R}^{2.7}$ as a function of rigidity R. The solid curve indicates the fit of Eq. (3) to the data. For illustration, the dashed curve uses the same fit values but with $\Delta\gamma$ set to zero. (b) The dependence of the proton flux spectral index γ on rigidity R.

incompatible with a single spectral index at the 99.9% C.L. The fit is shown in Fig. 4(a). For illustration, the fit results with $\Delta\gamma$ set to zero are also shown in Fig. 4(a).

To obtain the detailed variation of γ with rigidity in a model independent way, the spectral index is calculated from

$$\gamma = d[\log(\Phi)]/d[\log(R)] \tag{4}$$

over independent rigidity intervals above 8.48 GV, see Ref. [25], with a variable width to have sufficient sensitivity to determine γ. The results are presented in Fig. 4(b). As seen in Fig. 4(b), the spectral index varies with rigidity. In particular, the spectral index progressively hardens with rigidity above ~100 GV.

In conclusion, knowledge of the rigidity dependence of the proton flux is important in understanding the origin, acceleration, and propagation of cosmic rays. Previous measurements of the proton flux in cosmic rays have reported different variations of the flux with energy and this has generated many theoretical models. Our precise measurement of the proton flux from 1 GV to 1.8 TV is based on 300 million events and detailed studies of the systematic errors. The flux deviates from a single power law and progressively hardens at high rigidities.

We thank former NASA Administrator Daniel S. Goldin for his dedication to the legacy of the ISS as a scientific laboratory and his decision for NASA to fly AMS as a DOE payload. We also acknowledge the continuous support of the NASA leadership including Charles Bolden and William Gerstenmeier and of the JSC and MSFC flight control teams which has allowed AMS to operate optimally on the ISS for over three years. We are grateful for the support of Jim Siegrist and Michael Salamon of the DOE. We also acknowledge the continuous support from MIT and its School of Science, Michael Sipser, Marc Kastner, Ernest Moniz, and Richard Milner. Research supported by: São Paulo Research Foundation (FAPESP) Grants No. 2014/19149-7 and No. 2014/50747-8, Brazil; CAS, NSFC, MOST, NLAA, the provincial governments of Shandong, Jiangsu, Guangdong, and the China Scholarship Council, China; the Finnish Funding Agency for Innovation (Tekes) Grants No. 40361/01 and No. 40518/03 and the Academy of Finland Grant No. 258963, Finland; CNRS, IN2P3, CNES, Enigmass, and the ANR, France; J. Trümper, J. D. Woerner, and DLR and Forschungszentrum Jülich under Project No. JARA0052, Germany; INFN and ASI, Italy, including the work of J. Bazo, D. D'Urso, F. Nozzoli, C. Pizzolotto, and V. Vitale at the ASI Science Data Center under ASI-INFN Agreements No. C/011/11/1 and No. 2014-037-R.0, work at INFN Sezioni di Bologna, Milano-Bicocca, Perugia, Pisa, Roma, and Trento under ASI-INFN Contracts No. I/002/13/0 and No. 2013-002-R.0; Grants No. NRF-2009-0080142 and No. NRF-2012-010226 at CHEP, Kyungpook National University and No. NRF-2013-004883 at Ewha Womans University, Korea; the Consejo Nacional de Ciencia y Tecnología at UNAM, Mexico; CIEMAT, IAC, SEIDI MINECO, CDTI, and CPAN, Spain; the Swiss National Science Foundation (SNSF), federal and cantonal authorities, Switzerland; Academia Sinica and the Ministry of Science and Technology (MOST) under Grant No. 103-2682-M-008-002, former President of Academia Sinica Yuan-Tseh Lee and former Ministers of MOST, Maw-Kuen Wu and Luo-Chuan Lee, Taiwan; and the Turkish Atomic Energy Authority at METU, Turkey. We gratefully acknowledge the strong support from CERN, including Rolf-Dieter Heuer, and from the European Space Agency. We are grateful for important discussions with Barry Barish, Jonathan Ellis, Jonathan Feng, Igor Moskalenko, Steve Olsen, George Smoot, Michael Turner, Steven Weinberg, Frank Wilczek, and Arnold Wolfendale.

[a]Also at ASI, I-00133 Roma, Italy.
[b]Present address: CP3, Université catholique de Louvain, Belgium.
[c]Also at Xi'an Jiaotong University (XJTU), Xi'an 710049, China.
[d]Also at Sun Yat–Sen University (SYSU), Guangzhou 510275, China.

[e]Present address: SRON, Utrecht, Netherlands.
[f]Present address: at European Organization for Nuclear Research (CERN), CH-1211 Geneva 23, Switzerland.
[g]Also at Shandong University (SDU), Jinan, Shandong 250100, China.
[h]Also at Harbin Institute of Technology (HIT), Harbin 150001, China.
[i]Also at University of Science and Technology of China (USTC), Hefei 230026, China.
[j]Also at Università di Siena, I-53100 Siena, Italy.
[k]Also at Laboratoire dAnnecy-le-Vieux de Physique Théorique (LAPTh), CNRS and Université Savoie Mont Blanc, F-74941 Annecy-le-Vieux, France.
[l]Also at Nankai University, Tianjin 300071, China.
[m]Also at Beijing Normal University (BNU), Beijing 100875, China.
[n]Also at Southeast University (SEU), Nanjing 210096, China.

[1] See, for example, P. Blasi, Braz. J. Phys. **44**, 426 (2014); also Astron. Astrophys. Rev. **21**, 70 (2013).
[2] M. Ackermann *et al.*, Phys. Rev. Lett. **112**, 151103 (2014); M. Hareyama *et al.*, J. Phys. Conf. Ser. **31**, 159 (2006); M. Boezio *et al.*, Astropart. Phys. **19**, 583 (2003); E. Diehl, D. Ellithorpe, D. Muller, and S. P. Swordy, Astropart. Phys. **18**, 487 (2003); J. Alcaraz *et al.*, Phys. Lett. B **490**, 27 (2000); W. Menn *et al.*, Astrophys. J. **533**, 281 (2000); R. Bellotti *et al.*, Phys. Rev. D **60**, 052002 (1999); M. Boezio *et al.*, Astrophys. J. **518**, 457 (1999); K. Asakimori *et al.*, Astrophys. J. **502**, 278 (1998); M. Ichimura *et al.*, Phys. Rev. D **48**, 1949 (1993); I. P. Ivanenko *et al.*, in *Proceedings of the 23rd International Cosmic Ray Conference, Calgary* (World Scientific, Singapore, 1993), p. 17.
[3] For the ATIC experiment see A. D. Panov *et al.*, Bull. Russ. Acad. Sci. Phys. **73**, 564 (2009); extracted from D. Maurin, F. Melot, and R. Taillet, Astron. Astrophys. **569**, A32 (2014).
[4] We are grateful to the BESS-Polar Collaboration for providing the BESS-Polar II proton spectrum, measured during a 25-day Antarctic balloon flight in December 2007 and January 2008. Statistical and systematic errors are combined. A publication detailing these measurements is in preparation. For a description of the BESS-Polar experiment see K. Abe *et al.*, Phys. Rev. Lett. **108**, 051102 (2012). For the BESS experiment see Y. Shikaze *et al.*, Astropart. Phys. **28**, 154 (2007); S. Haino *et al.*, Phys. Lett. B **594**, 35 (2004); T. Sanuki *et al.*, Astrophys. J. **545**, 1135 (2000).
[5] For the CREAM experiment see Y. S. Yoon *et al.*, Astrophys. J. **728**, 122 (2011).
[6] For the PAMELA experiment see O. Adriani *et al.*, Astrophys. J. **765**, 91 (2013); Science **332**, 69 (2011).
[7] See, for example, G. Bernard, T. Delahaye, P. Salati, and R. Taillet, Astron. Astrophys. **555**, A48 (2013); V. S. Ptuskin, V. Zirakashvili, and E. S. Seo, Astrophys. J. **763**, 47 (2013); N. Tomassetti, Astrophys. J. Lett. **752**, L13 (2012); P. Blasi, E. Amato, and P. D. Serpico, Phys. Rev. Lett. **109**, 061101 (2012); A. E. Vladimirov, G. Jóhannesson, I. V. Moskalenko, and T. A. Porter, Astrophys. J. **752**, 68 (2012).
[8] A. Kounine, Int. J. Mod. Phys. E **21**, 1230005 (2012); S. Rosier-Lees, in Proceedings of Astroparticle Physics TEVPA/IDM, Amsterdam, 2014 (to be published); S. Ting, Nucl. Phys. B, Proc. Suppl. **243–244**, 12 (2013); S.-C. Lee, in Proceedings of the 20th International Conference on Supersymmetry and Unification of Fundamental Interactions (SUSY 2012), Beijing, 2012 (unpublished); M. Aguilar, in Proceedings of the XL International Meeting on Fundamental Physics, Centro de Ciencias de Benasque Pedro Pascual, 2012 (unpublished); S. Schael, in Proceedings of the 10th Symposium on Sources and Detection of Dark Matter and Dark Energy in the Universe, Los Angeles, 2012 (unpublished); B. Bertucci, *Proc. Sci.*, EPS-HEP (2011) 67; M. Incagli, AIP Conf. Proc. **1223**, 43 (2010); R. Battiston, Nucl. Instrum. Methods Phys. Res., Sect. A **588**, 227 (2008).
[9] K. Lübelsmeyer *et al.*, Nucl. Instrum. Methods Phys. Res., Sect. A **654**, 639 (2011).
[10] B. Alpat *et al.*, Nucl. Instrum. Methods Phys. Res., Sect. A **613**, 207 (2010).
[11] V. Bindi *et al.*, Nucl. Instrum. Methods Phys. Res., Sect. A **743**, 22 (2014) and references therein.
[12] J. Allison *et al.*, IEEE Trans. Nucl. Sci. **53**, 270 (2006); S. Agostinelli *et al.*, Nucl. Instrum. Methods Phys. Res., Sect. A **506**, 250 (2003).
[13] J. Alcaraz *et al.*, Phys. Lett. B **484**, 10 (2000); see also Ref. [16].
[14] C. C. Finlay *et al.*, Geophys. J. Int. **183**, 1216 (2010).
[15] P. Papini *et al.*, Astrophys. J. **615**, 259 (2004).
[16] M. Aguilar *et al.*, Phys. Rep. **366**, 331 (2002).
[17] The AMS Collaboration, Measurement of the Flux of Helium Nuclei in Primary Cosmic Rays with the Alpha Magnetic Spectrometer on the International Space Station, (to be published), will include a detailed comparison of the flux of protons and helium nuclei. Our measured helium flux spectral index as a function of rigidity is different than our proton spectral index; The AMS Collaboration, Measurement of the Flux of Light Nuclei in Primary Cosmic Rays with the Alpha Magnetic Spectrometer on the International Space Station (to be published).
[18] M. Aguilar *et al.*, Phys. Rev. Lett. **113**, 121102 (2014).
[19] G. D'Agostini, Nucl. Instrum. Methods Phys. Res., Sect. A, **362**, 487 (1995); V. Blobel, Report No. DESY-84-118, 1984; A. Kondor, Nucl. Instrum. Methods Phys. Res., **216**, 177 (1983).
[20] J. Albert *et al.*, Nucl. Instrum. Methods Phys. Res., Sect. A **583**, 494 (2007).
[21] IGRF-12 (2015), currently available at http://www.ngdc.noaa.gov/IAGA/vmod/igrf.html (unpublished).
[22] P. Bobik, G. Boella, M. J. Boschini, D. Grandi, M. Gervasi, K. Kudela, S. Pensotti, and P. G. Rancoita, J. Geophys. Res. **111**, A05205 (2006); N. A. Tsyganenko and M. I. Sitnov, J. Geophys. Res. **110**, A03208 (2005).
[23] N. Abgrall *et al.*, Phys. Rev. C **84**, 034604 (2011); J. R. Letaw, R. Silberberg, and C. H. Tsao, Astrophys. J. Suppl. Ser. **51**, 271 (1983); A. S. Carroll *et al.*, Phys. Lett. **80B**, 319 (1979); S. P. Denisov, S. V. Donskov, Yu. P. Gorin, R. N. Krasnokutsky, A. I. Petrukhin, Yu. D. Prokoshkin, and D. A. Stoyanova, Nucl. Phys. **B61**, 62 (1973); G. Bellettini, G. Cocconi, A. N. Diddens, E. Lillethun, G. Matthiae, J. P. Scanlon, and A. M. Wetherell, Nucl. Phys. **79**, 609 (1966); T. Bowen, M. Di Corato, W. H. Moore, and G. Tagliaferri, Il Nuovo Cimento **9**, 908 (1958).

[24] L. Accardo *et al.*, Phys. Rev. Lett. **113**, 121101 (2014); M. Aguilar *et al.*, Phys. Rev. Lett. **110**, 141102 (2013).

[25] See Supplemental Material at http://link.aps.org/supplemental/10.1103/PhysRevLett.114.171103 for the tabulated flux.

[26] A progress report on our proton analysis was presented at the 33rd International Cosmic Ray Conference (2013). At that time, our understanding of the systematic errors did not allow an accurate determination of the behavior of the proton flux.

[27] G. D. Lafferty and T. R. Wyatt, Nucl. Instrum. Methods Phys. Res., Sect. A **355**, 541 (1995). We have used Eq. (6) with $\tilde{R} \equiv x_{lw}$.

[28] L. J. Gleeson and W. I. Axford, Astrophys. J. **154**, 1011 (1968).

[29] We have chosen this particular equation, which is a double power law with a transition between low rigidity and high rigidity power laws, as it describes our data well. This function has been widely used for many years to describe different physics phenomena, see for example Eq. (1), K. Beuermann *et al.*, Astron. Astrophys. **352**, L26 (1999) and Eq. (43), L. Hernquist, Astrophys. J. **356**, 359 (1990).

[30] I. G. Usoskin, G. A. Bazilevskaya, and G. A. Kovaltsov, J. Geophys. Res. **116**, A02104 (2011); K. G. McCracken and J. Beer, J. Geophys. Res. **112**, A10101 (2007); I. G. Usoskin, K. Alanko-Huotari, G. A. Kovaltsov, and K. Mursula, J. Geophys. Res. **110**, A12108 (2005). We have also used more recent data from: http://cosmicrays.oulu.fi/phi/Phi_mon.txt.